ELSEVIER

Chemical Engineering Journal 71 (1998) 183–189

Chemical Engineering Journal

Numerical study of natural convection in Czochralski crystallization

Xiaobo Wu[a], Koichi Kakimoto[a], Hiroyuki Ozoe[a,*], Zengyue Guo[b]

[a] *Institute of Advanced Material Study, Kyushu University, Kasuga, Fukuoka 816, Japan*
[b] *Department of Engineering Mechanics, Tsinghua University, Beijing 100084, China*

Received 8 April 1997; received in revised form 22 April 1998; accepted 6 May 1998

Abstract

Natural convection in the melt phase of the Czochralski crystal growth system is unavoidable due to the gravitational field. Both horizontal and vertical temperature gradients influence the stability of the melt convection. For a tall crucible, a boundary layer type of convection is dominant, while Rayleigh–Benard-type convection occurs for a shallow crucible. A low Reynolds number κ–ε model was employed, but found to be inadequate for prediction and a more sophisticated model is required.

Keywords: Natural convection; Czochralski crystallization; Melt phase

1. Introduction

The Czochralski method is widely used to produce single crystal rods with a large diameter that is preferred for the manufacture of electronic and optical devices. Since the crystal rods are formed by solidification of the melt, convection has significant effects on their quality. It is known that fluctuations of the flow and temperature in the melt cause inhomogeneous distribution of dopants and/or crystal structure, which is generally referred as 'striation.'

Fluctuations of temperature in the melt have been confirmed by experiments and direct observations. Iliev et al. [1] measured the temperature fluctuations of the melt with thermocouples, while Edwell et al. [2] measured oscillations in temperature by using optical fibers. Munakata and Tanasawa [3] and Ozoe et al. [4] reported oscillatory characteristics of the melt in a Czochralski configuration system similar to that considered herein, while Kakimoto et al. [5] directly measured particle paths in the Si melt with a sophisticated X-ray topography technique. The current status of the research on flow instability in the melt has been reviewed by Muller [6] and by Ristorcelli and Lumley [7]. However, the prediction and control of such instability are still under investigation.

Instability is one of the active branch in the field of fluid mechanics. The study of instability of Benard convection [8,9] has been mostly limited to simple geometries. Recently, with the development of computer technology and numerical methods of simulation it has become possible to explore the unstable structure of the flow by solving nonlinear transient momentum and energy equations, including the Hoph point [10].

The present paper considers the influence on the Czochralski system of many parameters such as the Reynolds numbers for rotation of the crystal and crucible, the Pandtl number of the melt, the Grashof number, the aspect ratio of the crucible, the ratio of the crucible to the radius of the crystal, the Marangoni number, etc. Due to the vertical and horizontal temperature gradients in the melt under the gravitational field, natural convection is unavoidable in a practical system for crystal growth. The purpose of this paper is to study the instability induced by natural convection in the Czochralski configuration. As the melt level changes while the crystal is pulled up from the melt, the aspect ratio of the melt changes. The time-averaged value of the convection predicted by low Reynolds κ–ε turbulent model is presented here.

2. Mathematical model and numerical method

A Czochralski bulk-flow model [11] is adopted to exhibit the physical mechanism of the present problem, while the shape of the crystal/melt interface and free surface of the melt are assumed to be a horizontal plane as shown in Fig. 1. Buoyancy is the only driving force considered in the present study.

*Corresponding author. Fax: +81-92-583-7838; e-mail: ozoe@cm.kyushu-u.ac.jp

1385-8947/98/$ – see front matter
PII: S1385-8947(98)00114-4

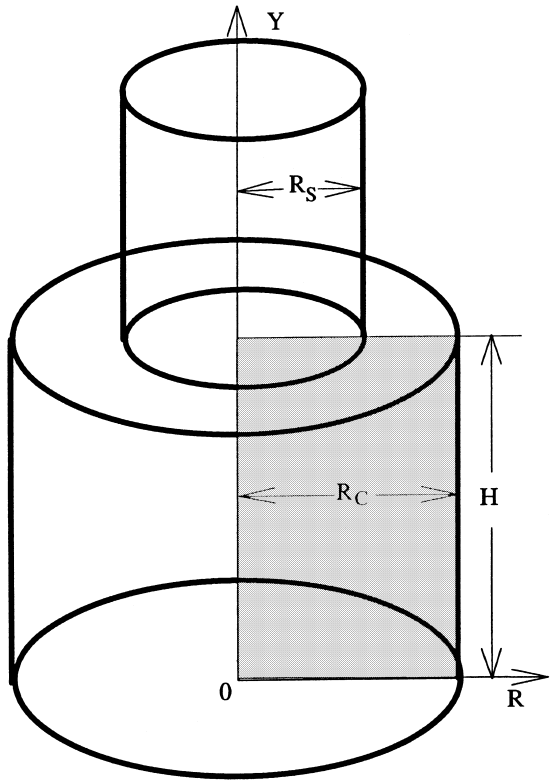

Fig. 1. Schematic of the Czochralski system and the coordinates.

As the Rayleigh number increases, natural convection in the melt successively experiences laminar, time-dependent and even turbulent states. The Navier–Stokes equation and energy equation may be used directly for the laminar and time-dependent regimes. To bridge the laminar and turbulent regimes, the low Reynolds number κ–ε model by Launder and Sharma [12] was also adopted to predict the Reynolds stress terms in the time-averaged equations of momentum and energy.

These differential equations and boundary conditions are written in dimensionless form with the following reference quantities: $L_r=R_c$ for length, $V_r=(g\beta R_c\Delta T)^{1/2}$ for velocity, $K_r=V_r^2$ for turbulent kinetic energy, and $\varepsilon_r=\nu K_r/R_c^2$ for turbulent kinetic energy dissipation rate, $\nu_r=\nu$ for effective viscosity, and $\theta=(T-T_m)/(T_W-T_m)$ for dimensionless temperature. The derived dimensionless parameters representing geometrical effects, fluid properties and relative magnitude of the driving force are:

$$\mathrm{Re}=\mathrm{Gr}^{1/2}$$

$$\mathrm{Gr}=g\beta\Delta TR_c^3/\nu^2$$

$$\mathrm{Pr}=\nu/\alpha$$

$$\mathrm{Ar}=H/R_c$$

$$\rho_R=R_s/R_c$$

With the above assumptions and scaling, the generalized equation governing the flow and heat transfer of the melt for both laminar and turbulent flow is:

$$\frac{\partial\phi}{\partial\tau}+\frac{1}{R}\frac{\partial}{\partial R}(RU\phi)+\frac{\partial}{\partial Y}(V\phi)=\frac{1}{R}\frac{\partial}{\partial R}\left(\Gamma_\phi R\frac{\partial\phi}{\partial R}\right)+\frac{\partial}{\partial Y}\left(\Gamma_\phi\frac{\partial\phi}{\partial Y}\right)+S_\phi \quad (1)$$

Table 1 lists the diffusion coefficient Γ_ϕ and source term S_ϕ for the generalized dependent variable ϕ. For laminar flow, the turbulent viscosity is set to zero. The boundary conditions for the problem are as follows:

$$Y=0;\ 0\le R\le 1:\quad U=V=\kappa^*=\xi^*=0;\ \theta=1$$

$$0\le Y\le \mathrm{Ar};\ R=1:\quad U=V=\kappa^*=\varepsilon^*=0;\ \theta=1$$

$$Y=\mathrm{Ar};\ 0\le R\le\rho_R\quad U=V=\kappa^*=\varepsilon^*=0;\ \theta=0$$

$$Y=\mathrm{Ar};\ \rho_R\le R\le 1\quad V=0;\ \frac{\partial U}{\partial Y}=\frac{\partial\theta}{\partial Y}=\frac{\partial\kappa^*}{\partial Y}=\frac{\partial\varepsilon^*}{\partial Y}=0$$

Table 1
The diffusion coefficient Γ_Φ and source term S_Φ for variable Φ

Φ	Γ_Φ	S_Φ
1	0	0
U	$\frac{1+\mu_t^*}{\mathrm{Re}}$	$-\frac{\partial P}{\partial R}+\frac{1}{R}\frac{\partial}{\partial R}\left(\frac{1+\mu_t^*}{\mathrm{Re}}R\frac{\partial U}{\partial R}\right)+\frac{\partial}{\partial Y}\left(\frac{1+\mu_t^*}{\mathrm{Re}}\frac{\partial V}{\partial R}\right)-\frac{2\mu_t^*}{R^2\mathrm{Re}}U$
V	$\frac{1+\mu_t^*}{\mathrm{Re}}$	$-\frac{\partial P}{\partial Y}+\frac{\partial}{\partial Y}\left(\frac{1+\mu_t^*}{\mathrm{Re}}\frac{\partial V}{\partial Y}\right)+\frac{1}{R}\frac{\partial}{\partial R}\left(\frac{1+\mu_t^*}{\mathrm{Re}}R\frac{\partial U}{\partial Y}\right)-\frac{\mathrm{Gr}}{\mathrm{Re}^2}\theta$
θ	$\frac{1}{\mathrm{Re}}\left(\frac{1}{Pr}+\frac{\mu_t^*}{\sigma_\theta}\right)$	0
κ^*	$\frac{1}{\mathrm{Re}}\left(1+\frac{\mu_t^*}{\sigma_\kappa}\right)$	$P_\kappa+G_\kappa+D-\varepsilon^*/\mathrm{Re}$
ε^*	$\frac{1}{\mathrm{Re}}\left(1+\frac{\mu_t^*}{\sigma_\varepsilon}\right)$	$\frac{\varepsilon^*}{\kappa^*}\left[C_{1\varepsilon}f_1(P_\kappa+C_{3\varepsilon}G_\varepsilon)-C_{2\varepsilon}f_2\frac{\varepsilon^*}{\mathrm{Re}}\right]+E$

$$P_\kappa=\frac{\mu_t^*}{\mathrm{Re}}\left\{2\left[\left(\frac{\partial U}{\partial R}\right)^2+\left(\frac{\partial V}{\partial Y}\right)^2+\left(\frac{U}{R}\right)^2\right]+\left(\frac{\partial U}{\partial Y}+\frac{\partial V}{\partial R}\right)^2\right\},\quad D=-\frac{2}{\mathrm{Re}}\left[\left(\frac{\partial\sqrt{\kappa^*}}{\partial R}\right)^2+\left(\frac{\partial\sqrt{\kappa^*}}{\partial Y}\right)^2\right],\quad G_\kappa=-\frac{\mu_t^*}{\sigma_\theta}\frac{Gr}{\mathrm{Re}^3}\frac{\partial\theta}{\partial Y}$$

$$E=\frac{2\mu_t^*}{\mathrm{Re}}\left[\left(\frac{\partial^2U}{\partial Y^2}\right)^2+\left(\frac{\partial^2V}{\partial R^2}\right)^2\right],\quad \mu_t^*=\frac{\mu_t}{\mu}=\mathrm{Re}^2C_\mu f_\mu\rho^*\frac{\kappa^{*2}}{\varepsilon^*},\quad \mathrm{Re}_t=\mathrm{Re}^2\kappa^{*2}/\varepsilon^*$$

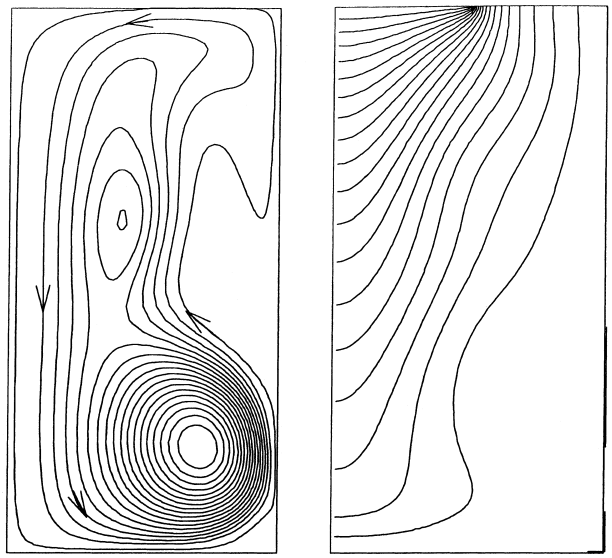

(a) Streamlines (b) Isotherms

Fig. 2. Steady laminar natural convection for Ra=3×10^4.

The governing equations and boundary conditions for the flow and heat transfer were solved numerically by the control-volume method. A staggered grid system was used to calculate the velocity field in the melt, and pressure and velocity were linked by the SIMPLEC [13] algorithm. The uniform grid 25×50 with a time step of 0.02 was employed for the calculation of laminar flow. For turbulent flow, a non-uniform grid 80×80 was used with a very dense mesh near the wall to account for the dramatical change of variables from the boundary to the core. The computation was assumed to have converged when the residues of all variables were less than 10^{-4}.

3. Results and discussion

3.1. Laminar steady flow

When the Rayleigh number is less than some critical value, the flow is steady and laminar. Fig. 2 shows the

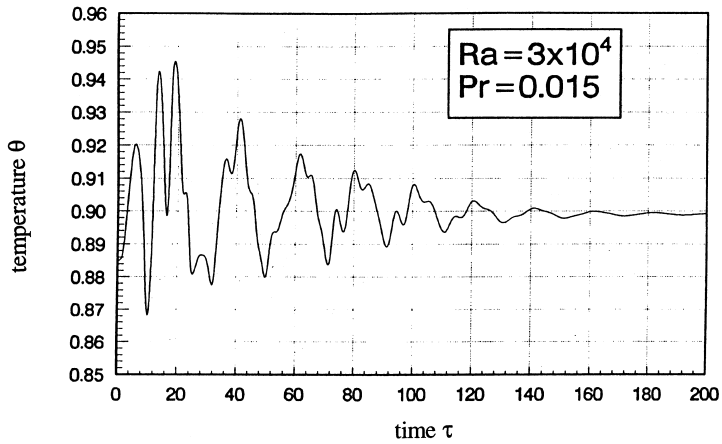

Fig. 3. Transient change of temperature at (R=0.5, Y=1) for Ra=3×10^4 and Pr=0.015.

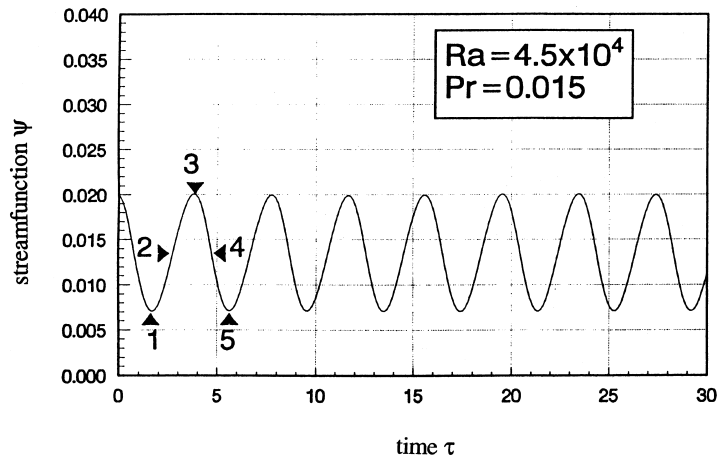

Fig. 4. Transient change of stream function at (R=0.5, Y=1) for Ra=4.5×10^4 and Pr=0.015.

streamlines and isothermal profiles at Ra=3×10^4 and Pr=0.015. The melt is heated along the wall of the crucible and cooled at the melt/crystal interface, which results in an anticlockwise circulating buoyancy-driven flow. For low Reynolds numbers, the flow is steady and as shown in Fig. 3, any disturbance is damped. However, the Rayleigh number for conventional Czochralski crystal growth is in the range between $9\times10^4-1.35\times10^6$.

3.2. Time-dependent flow

When the Rayleigh number increases, the flow first undergoes a bifurcation to an unsteady, periodic solution. The flow structure may become more complex with several vortices in the melt. Fig. 4 shows the variation of the stream function with time at the location R=0.5 and Y=1 for Rayleigh number of 4.5×10^4 and a Prandtl number of

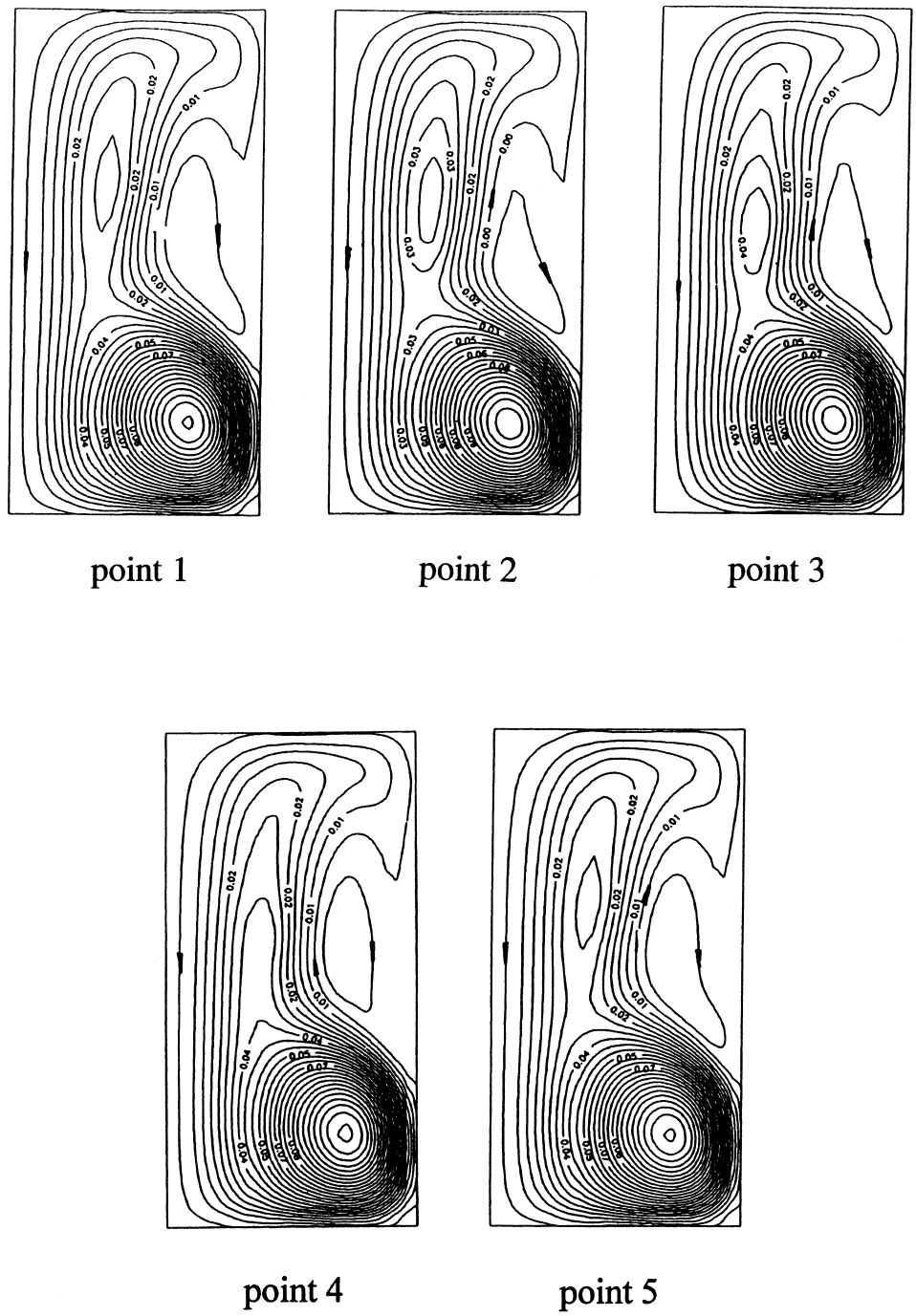

Fig. 5. Streamline perturbation over one period of the oscillation corresponding to the marked point in Fig. 4.

0.015. The value of the stream function oscillates periodically without damping. Fig. 5 shows a series of instantaneous streamlines of the melt in one cycle of the oscillation. The flow pattern changes periodically, although it is quite limited in its magnitude.

For natural convection in a Czochralski configuration, two types of instability may be noted. One is the boundary layer-type of instability due to the horizontal temperature gradient along the vertical wall of a crucible, and the other is related to the Rayleigh–Benard-type instability of the region heated from below, in this case, the bottom of the crucible. These instabilities are dependent on the aspect ratio of the melt. For a tall crucible (large aspect ratio), which represents the initial stage of crystal growth, the flow is dominated by the boundary-layer-type, such as those of Fig. 5. As the aspect ratio decreases, the flow structure becomes like that in Fig. 6. In Fig. 6(a), the flow is separated along the vertical wall of the crucible. Fig. 6(b) shows the flow pattern of the melt with an aspect ratio 0.5. However, with further decrease in the aspect ratio of the melt as occurs in the tail-end stage, a Rayleigh–Benard-type flow is found, as shown in Fig. 6(c). These characteristics are summarized in Fig. 7. The ordinate is a critical Rayleigh number for the start of oscillatory convection. The peak value is found at an aspect ratio of 0.5. Flow is dominated by the boundary-layer-type of instability when the aspect ratio is greater than 0.5 and by the Rayleigh–Benard-type instability when the aspect ratio is less than that value.

3.3. Towards turbulent flow

In a large-scale Czochralski crystal growth system, the non-dimensional parameters such as the Reynolds number, the Grashof number, etc. become large, which implies that the melt flow may become turbulent. Several researchers [14–16] have employed the turbulent model to solve the flow structure of the melt in a Czochralski system. Here, emphasis is put on the flow behavior of natural convection using a low Reynolds number κ–ε model.

Fig. 8 shows the dimensionless streamlines, isotherms and turbulent viscosity at a Rayleigh number of $Ra=2\times10^8$ and an aspect Ar=2. Compared with the laminar time-dependent flow of Fig. 5, no separation is found along the vertical wall of the crucible, and one vortex is formed in the melt, which is similar to the result of Kinney and Brown [14] who implemented a hybrid κ–ε model. For a shallow crucible, however, both κ and ε decreased to zero

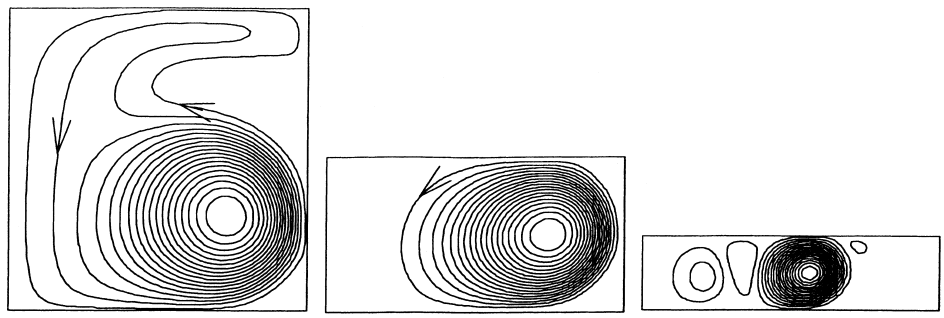

Fig. 6. Variation of flow pattern with aspect ratio for $Ra=2.25\times10^5$.

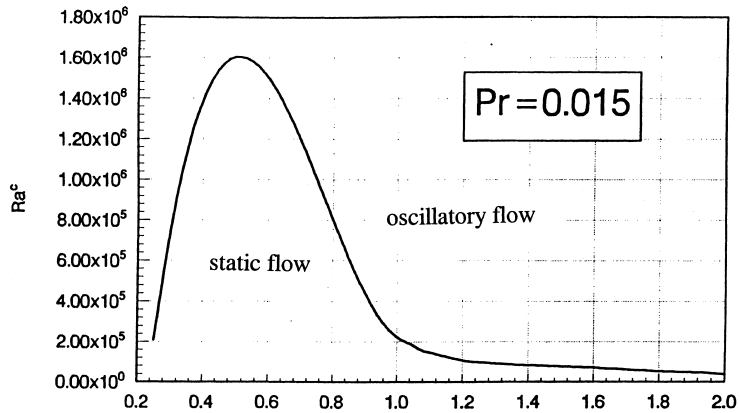

Fig. 7. Variation of critical Rayleigh number with aspect ratio.

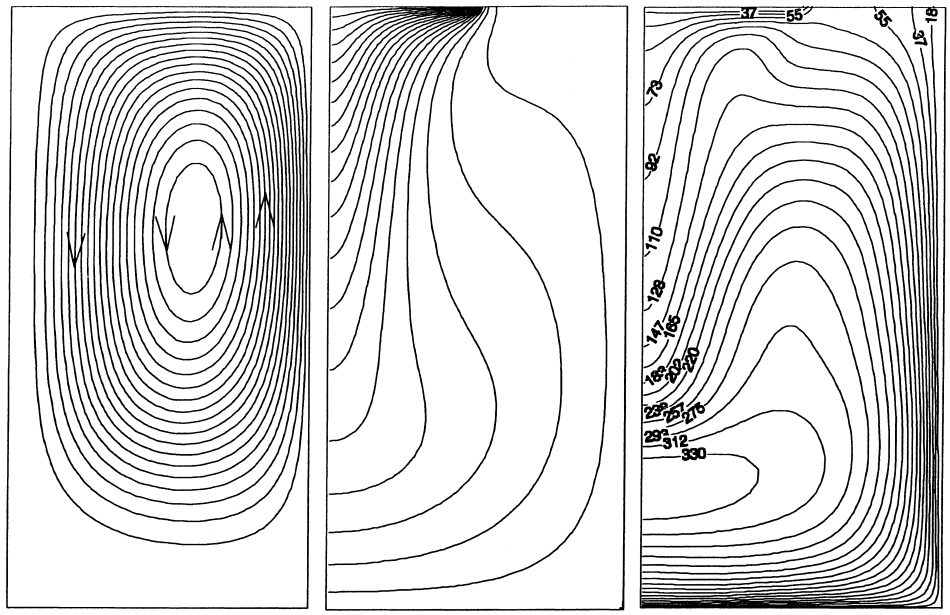

Fig. 8. Turbulent natural convection computed by low Reynolds κ–ε model at Ra=2×10^8.

during the process of computation, resulting in a zero-turbulent viscosity within the melt. A similar result is also demonstrated by Hanjalic [17] for natural convection in a horizontal enclosure heated from below.

This suggests that the low Reynolds number κ–ε model yields only one-vortex structures that may overpredict turbulent viscosity in some regions. For practical Czochralski crystal growth, the melt flow may be more complicated due to other driving forces, and a more sophisticated turbulent model may be required to produce realistic results.

The numerical results, both laminar and turbulent, have been known to depend on grid sizes. The present computations were carried out for laminar and/or turbulent flows, with uniform or non-uniform grids, respectively. Although we did not carry out the detailed study on the effect of grid sizes, substantively different results are not expected according to our previous computational experiences on this point.

4. Conclusion

Natural convection in a Czochralski configuration was analyzed numerically. Both laminar and low-Reynolds number κ–ε models were employed.

1. When the Rayleigh number of the melt is less than some critical value, the flow is steady.
2. The aspect ratio of the melt significantly influences mode of flow of the melt convection. For a tall crucible, convection is dominated by boundary layer-type of flow; for a shallow layer, convection is dominated by Rayleigh–Benard-type flow.
3. A low Reynolds number κ–ε turbulent model was employed for natural convection. It predicted only one vortex, which is the result of overprediction of turbulent viscosity. For a shallow crucible, the value of turbulent variables decreases to zero, resulting in laminar convection.

5. Nomenclature

Ar	aspect ratio=H/R_c
g	acceleration due to gravity (m s^{-2})
Gr	Grashof number=$g\beta\Delta T\, R_c^3/\nu^2$
H	height of the melt (m)
P	dimensionless pressure=$p/\rho V_r^2$
Pr	Prandt1 number=ν/α
R	dimensionless radial coordinate=r/R_c
Ra	Rayleigh number Ra=Gr·Pr
R_c	inner radius of the crucible (m)
R_s	radius of the crystal (m)
Re	equivalent Reynolds number=$\sqrt{\text{Gr}}$
S	source term
t	time (s)
t_r	referent time=R_c/V_r
T	temperature (K)
U	dimensionless radial velocity=u/V_r
V	dimensionless axial velocity=v/V_r
Y	dimensionless axial coordinate=y/R_c

5.1. Greek symbols

α thermal diffusivity ($m^2\ s^{-1}$)
κ turbulent kinetic energy ($m^2\ s^{-2}$)
ε turbulent energy dissipation ($m^2\ s^{-3}$)
ϕ general dependent variable
β volumetric coefficient of expansion with temperature (1/K)
λ thermal conductivity ($W\ m^{-1}\ K^{-1}$)
μ dynamic viscosity ($kg\ m^{-1}\ s^{-1}$)
ν kinetic viscosity=μ/ρ ($m^2\ s^{-1}$)
ρ density ($kg\ m^{-3}$)
ρ_s ratio of the crystal radius to the crucible radius=R_s/R_c
θ dimensionless temperature $(T-T_m)/(T_W-T_m)$
τ dimensionless time=t/t_r
Γ diffusion coefficient

5.2. Subscript

c crucible
r reference
s crystal
t turbulent

5.3. Superscript

c critical
* dimensionless

References

[1] K. Iliev, M. Berkowski, V. Nikolov, P. Peshv, W. Piekarczyk, Conditions of existence and character of the temperature fluctuations during Czochralski growth of oxide single crystal, J. Crystal Growth 118 (1991) 219–224.
[2] D. Edwill, E. Andersen, R.R. Dils, Temperature oscillation in silicon melts, J. Crystal Growth 98 (1989) 667–678.
[3] T. Munakata, I. Tanasawa, Onset of oscillatory flow in a Czochralski growth melt and its suppression by magnetic field, J. Crystal Growth 106 (1990) 566–576.
[4] H. Ozoe, K. Toh, T. Inoue, Transition mechanism of flow mode in Czochralski convection, J. Crystal Growth 110 (1991) 472–480.
[5] K. Kakimoto, M. Watanabe, T. Hibiya, Direct observation by X-ray radiography of convection of molten silicon in the Czochralski growth method, J. Crystal Growth 88 (1988) 365.
[6] G. Muller, Convection instabilities in melt growth configuration, J. Crystal Growth 128 (1993) 26–36.
[7] R.R. Ristorcelli, J.L. Lumley, Instabilities, transition and turbulence in Czochralski crystal melt, J. Crystal Growth 116 (1992) 447–460.
[8] H. Benard, Les tourbillons cellulair dans nappe liquide transportant de la chaleur pur convections en regime permanent, Rev. Gen Sci. Pures Appl. Bull. Assoc. 11 (1900) 1261–1271, 1309–1328.
[9] P.C. Drazin, W.H. Reid, Hydrodynamic Instability, Cambridge University Press, Cambridge, 1981.
[10] G. Neumann, Three-dimensional numerical simulation of buoyancy-driven convection in vertical cylinders heated from below, J. Fluid Mech. 214 (1990) 559–578.
[11] M.J. Crochet, P.J. Wouters, Finite-element simulation of Czochralski flow, J. Crystal Growth 65 (1983) 153–165.
[12] B.E. Launder, B.I. Sharma, Application of the energy-dissipation model of turbulence to the calculation of flow near a spinning disc, Letter in Heat Mass Transfer 1 (1974) 131–138.
[13] J.P. Van, G.D. Raithby, Enhancement of the SIMPLE method for predicting incompressible fluid flow, Numerical Heat Transfer 7 (1984) 147–163.
[14] T.A. Kinney, R.A. Brown, Application of turbulence modeling to the integrated hydrodynamics thermal-capillary model of Czochralski crystal of silicon, J. Crystal Growth 132 (1993) 551–574.
[15] H.T. Chung, S.C. Lee, J.K. Yoon, Numerical prediction of operational parameters in Czochralski growth of large-scale Si, J. Crystal Growth 163 (1996) 246–258.
[16] N. Ono, M. Kida, Y. Arai, K. Sahira, A numerical study of oxygen transport in silicon melt in a double-crucible method, J. Crystal Growth 137 (1994) 427–434.
[17] K. Hanjalic, Achievements and limitations in modeling and computation of buoyant turbulent flows and heat transfer, 10th Int. Heat Transfer Conf., Brighton, UK, vol. 1, 1994, pp. 1–18.